Electronic band structure and Fermi surface of $Ag_5Pb_2O_6$

Tamio Oguchi
Department of Quantum Matter, ADSM, Hiroshima University, Higashihiroshima 739-8530, Japan
(Received 4 September 2005; revised manuscript received 18 October 2005; published 7 December 2005)

We present the electronic band structure of $Ag_5Pb_2O_6$ with layered hexagonal structure containing one-dimensional chains and two-dimensional kagomé layers of silver. A half-filled conduction band shows extremely simple, single nearly-free-electron-like Fermi surface. The conduction band is composed of an antibonding state of Pb 6*s* and O 2*p* mixing with Ag 4*d* and 5*s*. The mass enhancement in the state density at the Fermi energy is expected to be negligibly small by comparing with the specific-heat data. The calculated Fermi velocity is consistent with the small anisotropy observed in transport properties. Doping effects on the electronic structure are also discussed.

DOI: 10.1103/PhysRevB.72.245105 PACS number(s): 71.18.+y, 71.20.Ps, 72.15.Jf, 74.25.Jb

I. INTRODUCTION

The novel transport properties of oxide compounds have attracted much attention since the discovery of high-critical-temperature (T_c) superconductivity. Some perovskite manganites show colossal magnetoresistance,[1] and layered-structure cobaltates reveal large thermoelectric power.[2] It is widely believed that one-dimensional (1D) chains and/or two-dimensional (2D) layers consisting of transition-metal and oxygen ions play a crucial role in the electronic properties in most of the cases. Recently Yonezawa and Maeno have observed an anomalous T^2 dependence of the resistivity for single crystals of $Ag_5Pb_2O_6$.[3] $Ag_5Pb_2O_6$ has a hexagonal crystal structure with 1D chains and 2D kagomé layers of silver ions interleaved with honeycomb layers of PbO_6 octahedra. The T^2 behavior of the resistivity is seen along both directions parallel and perpendicular to the layers in a wide temperature range. Anisotropy is found to be rather small like a factor of 2 in the resistivity. The measured specific-heat γ value is just moderate, implying a small mass enhancement factor. Yonezawa and Maeno have concluded that the T^2 dependence cannot be interpreted by either the electron-electron interaction or electron-phonon mechanism. In addition, they have reported an indication of a superconducting phase below 48 mK, which has been confirmed by a resistivity measurement quite recently.[4] Concerning the electronic structure of $Ag_5Pb_2O_6$, Brennan and Burdett have calculated the density of states and Fermi surface within a tight-binding (TB) model.[5] It has been claimed that a carrier electron around the Fermi energy is delocalized over the entire silver 1D and 2D substructure. Recently, another band structure calculation has been reported with the full-potential linearized muffin-tin orbital method.[6] The obtained band structure of $Ag_5Pb_2O_6$ is qualitatively different from the previous TB one and quite consistent with a result of the present study, as will be shown below.

In this paper, we present the electronic band structure and Fermi surface of $Ag_5Pb_2O_6$ calculated by using a first-principles density-functional method. The calculated results show a basic electronic structure of $(Ag^+)_5(Pb^{4+})_2(O^{2-})_6 +(-e)$: namely, a single nearly-free-electron-like conduction band with one electron per formula unit appearing in energy gaps formed in an ionic crystal. Very interestingly, the conduction band is found to be a 2D antibonding state of Pb 6*s* and O 2*p* and its dispersion along the *c* direction originates in hybridization with Ag 4*d* and 5*s*, resulting in three-dimensional (3D) nearly-free-electron-like Fermi surface. In order to investigate transport properties, the Fermi velocity and Hall coefficients are evaluated from the obtained electronic band structure. Finally, doping effects for the Pb site on the electronic band structure are also discussed in detail.

II. CRYSTAL STRUCTURE

Crystal structure data of the hexagonal $Ag_5Pb_2O_6$ are taken from an experiment by Jansen and Heidebrecht,[7] as shown in Fig. 1. The space group is $P\bar{3}1m$ with lattice constants of $a=5.9324$ Å and $c=6.4105$ Å. Crystallographically independent atomic positions are given at $(0,0,z)$ with $z=0.2413$ for 1D-chain silver [denoted as Ag(1)], $(1/2,0,0)$ for 2D-layer silver [denoted as Ag(2)], $(2/3,1/3,1/2)$ for Pb, and $(x,0,z)$ with $x=0.6222$ and $z=0.6889$ for O. There are two sites for Ag(1), three for Ag(2), two for Pb, and six for O in a hexagonal unit cell. Typical interatomic distances

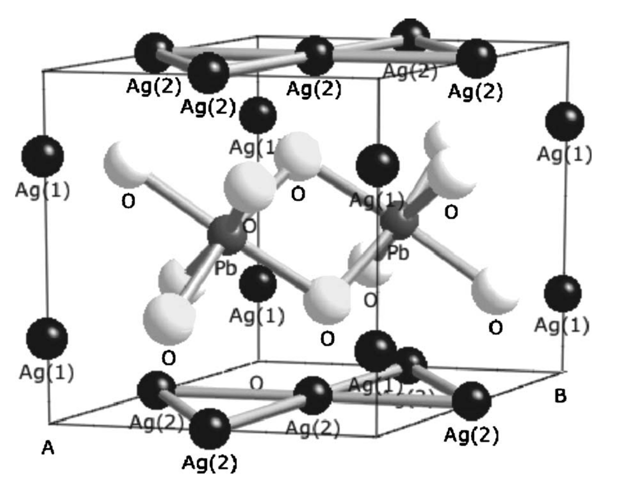

FIG. 1. Crystal structure of the hexagonal $Ag_5Pb_2O_6$. Dark, grey, and white spheres denote Ag, Pb, and O atomic sites, respectively.

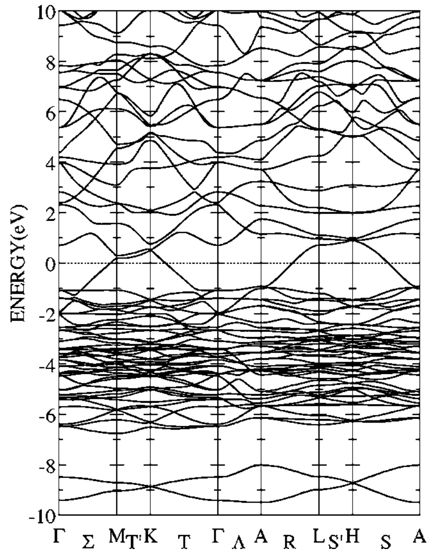

FIG. 2. Calculated energy band structure of the hexagonal $Ag_5Pb_2O_6$. The Fermi energy is taken at the origin.

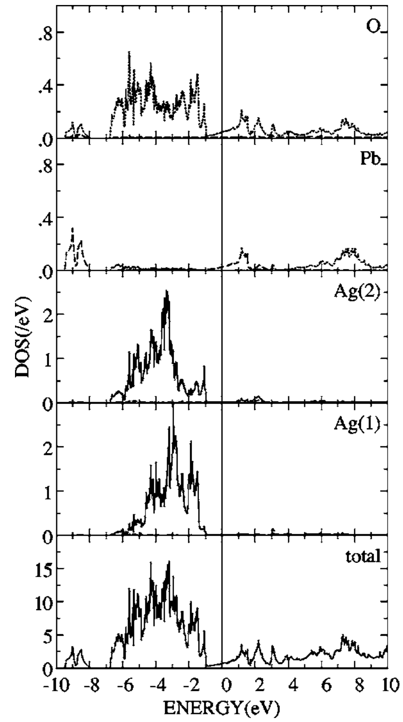

FIG. 3. Calculated total and partial density of states (DOS) of the hexagonal $Ag_5Pb_2O_6$. The Fermi energy is taken at the origin. Dashed, dotted, and solid lines represent s,p, and d angular momentum components, respectively, in the partial DOS.

are 3.094 Å for Ag(1)-Ag(1), 2.966 Å for Ag(2)-Ag(2), and 2.219 Å for Pb-O. It is quite important to note that the nearest atomic distances of Ag(1)-O and Ag(2)-O are 2.285 Å and 2.122 Å, respectively, which are both much closer than those of Ag(1)-Ag(1) and Ag(2)-Ag(2). Therefore, it is doubtful and unreliable to understand the electronic structure of $Ag_5Pb_2O_6$ only in terms of 1D chains and 2D layers of silver ions.

III. METHODS

The present first-principles calculations are based on the density-functional theory by adopting the all-electron full-potential linear-augmented-plane-wave (FLAPW) method.[8–10] Our implementation of the all-electron FLAPW method has been used successfully for a variety of condensed matter systems.[11–14] Self-consistent-field (SCF) calculations are performed with the scalar-relativistic scheme and the improved tetrahedron integration method[15] up to $16\times16\times16$ **k**-mesh points in the Brillouin zone (BZ). Muffin-tin sphere radii are assumed to be 1.1 Å for Ag, 1.0 Å for Pb, and 0.8 Å for O. Note that each partial density of states (DOS) shown below is projected on the corresponding partial spherical wave within the muffin-tin sphere. Exchange and correlation are treated within the local density approximation[16] (LDA) or generalized gradient approximation[17] (GGA). For the present $Ag_5Pb_2O_6$ with the observed crystal structure, the LDA and GGA give almost identical electronic band structure around the Fermi energy. We show only LDA results.

IV. RESULTS AND DISCUSSION

A. Electronic band structure

Figure 2 shows the calculated electronic band structure of hexagonal $Ag_5Pb_2O_6$ along several high-symmetry lines in the BZ. Each band dispersion is drawn according to its irreducible representation of the group of **k**. Two bands around −9 eV in Fig. 2 are mostly bonding states between Pb 6*s* and O 2*p* orbitals. Complex bands between −7 and −1 eV are composed of O 2*p* and Ag 4*d* orbitals mixed lightly with Pb 6*p* and Ag 5*s* as bonding states. A conduction band crossing the Fermi energy is dominated by an antibonding state of Pb 6*s* and O 2*p*, forming a single cylindrical Fermi surface warping along the *c* direction, as shown below. Those orbital components of each band can be seen more clearly in the angular-momentum-projected DOS shown in Fig. 3. In the upper part of the antibonding bands around +2 eV in Fig. 3, one can see a peak containing Ag(2) 4*d* and 5*s*, which is a similar structure to that found in the previously calculated DOS.[5] An important difference from the previous one is the existence of the antibonding band of Pb 6*s* and O 2*p* crossing the Fermi energy, which must govern the transport properties of the system. The Ag 4*d* and 5*s* orbitals also hybridize with the antibonding band to some extent, and the electron density at the Fermi energy is delocalized over the entire crystal. It is, therefore, summarized that the basic electronic band structure can be considered as $(Ag^{+})_5(Pb^{4+})_2(O^{2-})_6+(-e)$, where a conduction band forming a quasi-2D cylindrical Fermi surface with large warping is half occupied by one electron carrier.

In order to make sure of the origin of the conduction band, energy band structures are calculated for $\square_5Pb_2O_6$ and $Ag_5\square_2O_6$ ($\square$=vacancy) with the same crystal structure as $Ag_5Pb_2O_6$ and shown in Figs. 4 and 5, respectively. SCF calculations are performed for both fictitious systems by keeping charge neutrality. Horizontal dotted lines in Figs. 4

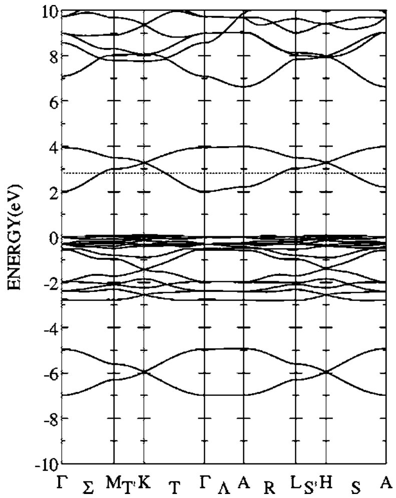

FIG. 4. Calculated energy band structure of $\square_5Pb_2O_6$ ($\square$=Ag vacancy). A horizontal dotted line represents the Fermi energy corresponding to $(\square^{+})_5(Pb^{4+})_2(O^{2-})_6+(-e)$.

and 5 represent a shifted Fermi energy by assuming $(\square^{+})_5(Pb^{4+})_2(O^{2-})_6+(-e)$ and $(Ag^{+})_5(\square^{4+})_2(O^{2-})_6+(-e)$ within the rigid-band approximation. It is reasonably understood that the conduction band crossing the Fermi energy in Fig. 2 originates in the lower branch of the antibonding bands of Pb 6*s* and O 2*p* in Fig. 4 by judging their dispersion. The more dispersive nature in Fig. 2 comes from the extra hybridization with the Ag orbitals, which is not involved in $\square_5Pb_2O_6$. The half-filled antibonding conduction band of Pb 6*s* and O 2*p* in Fig. 4 gives just a 2D Fermi surface with cylindrical shape and almost no warping along the *c* direction. The warping behavior in $Ag_5Pb_2O_6$ might come from the transfer integrals between Ag 4*d* and 5*s* and O 2*p* orbitals as shown in Fig. 5, in which a clear cosine dispersion ($\sim -\cos k_z c$) is seen along ΓA.

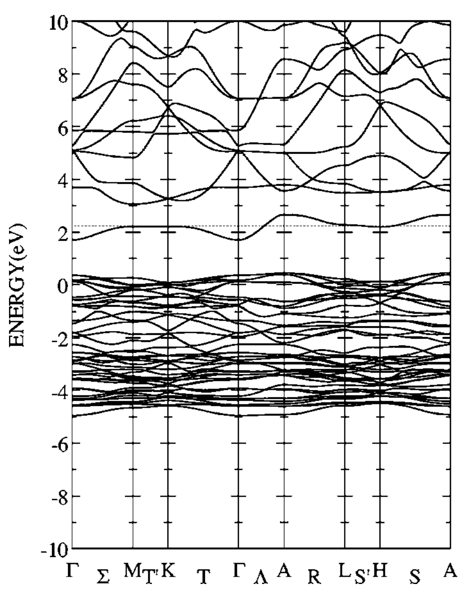

FIG. 5. Calculated energy band structure of $Ag_5\square_2O_6$ ($\square$=Pb vacancy). A horizontal dotted line represents the Fermi energy corresponding to $(Ag^{+})_5(\square^{4+})_2(O^{2-})_6+(-e)$.

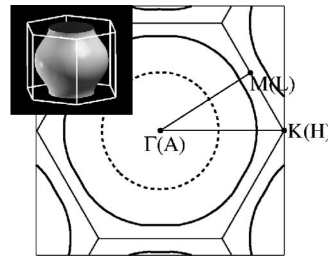

FIG. 6. Calculated Fermi surface of the hexagonal $Ag_5Pb_2O_6$. Solid and dotted lines denote the cross sections on the ΓMK ($k_z=0$) and ALH ($k_z=\pi/c$) planes in the BZ, respectively. The inset is a perspective view of the Fermi surface.

The calculated total DOS at the Fermi energy is 1.33 states/[eV (formula unit)]. This value corresponds to the electronic specific heat coefficient $\gamma=3.13$ mJ/(K^2 mol), which gives very small mass enhancement $\lambda=0.09$ by comparing with the experimental value $\gamma=3.42$ mJ/(K^2 mol).[3] The calculated Pauli paramagnetic susceptibility is $\chi_0=4.30\times10^{-5}$ emu/mol, which is also comparable with the experimental value $(+3.7\pm0.2)\times10^{-5}$ emu/mol. It might be hard to evaluate the Stoner enhancement from the comparison because the experimental χ_0 may have certain ambiguities due to significantly large diamagnetic contribution from the core electrons $(-2.44\times10^{-4}$ emu/mol).[3]

B. Fermi surface

The obtained band structure for $16\times16\times16$ **k**-mesh points (417 **k** points in the irreducible wedge of the BZ) is fitted with symmetrized star functions by a spline method and used for calculations of the Fermi surface and related properties.[18] Figure 6 shows the Fermi surface of the hexagonal $Ag_5Pb_2O_6$. The cross sections on the ΓMK ($k_z=0$) and ALH ($k_z=\pi/c$) planes in the BZ are almost circle, indicating cylindrical shape with large warping along the *c* direction. The Fermi wave numbers from the axis ΓA along ΓM, ΓK, AL, and AH are 0.543, 0.551, 0.331, and 0.332 Å^{-1}, respectively. The warping along the *c* direction is of almost perfect cosine shape, independent of the lateral components of the wave vector **k**. It is possible to look upon the Fermi surface as a nearly-free-electron-like spherical one deformed by overlapping the neighbors at the BZ boundaries of $k_z=\pm\pi/c$. Quantum-oscillation measurements such as de Haas–van Alphen (dHvA) and Shubnicov–de Haas effects are highly desired since the single crystal is available and can be compared with the present band-theoretical prediction to elucidate detailed information of the Fermi surface. By applying a magnetic field along the *c* direction, two quantum-oscillation signals should be observed around frequencies of 3.6 kT (cyclotron mass $m^*\approx0.68m$) and 9.8 kT ($m^*\approx1.2m$) associated with the extreme Fermi surface cross sections shown in Fig. 6. The large extreme cross section is nearly constant due to its fat belly shape at small polar angles, analogous to that expected for a spherical Fermi surface, and shows discontinuous features because of a warping geometry at larger angles than 60°. The small extreme cross section shows a strong angle dependence at intermediate po-

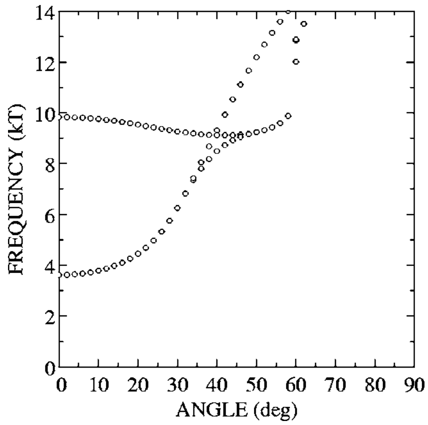

FIG. 7. Calculated de Haas–van Alphen frequencies for the Fermi surface of hexagonal $Ag_5Pb_2O_6$. The angle is taken as the polar direction of the magnetic field from [0001] to [1000].

lar angles and breaks up at 34° into two branches, of which one merges into the large one around 50°. The two extreme cross sections corresponding to the dHvA frequencies are depicted in Fig. 7 as a function of the polar angle of the applied magnetic field.

C. Transport properties

The calculated Fermi velocity is $\langle v_x^2\rangle^{1/2}=\langle v_y^2\rangle^{1/2}=3.57\times10^7$ cm/s and $\langle v_z^2\rangle^{1/2}=2.43\times10^7$ cm/s. According to the Boltzmann theory, the dc conductivity is proportional to the Fermi velocity squared with the constant relaxation-time approximation. The ratio $\langle v_x^2\rangle/\langle v_z^2\rangle\approx2.16$ may explain the small anisotropy of the observed resistivity $\rho_c/\rho_{ab}\approx2$ at 280 K,[3] where isotropic diffusive scattering is dominant. In Sr_2RuO_4 and high-T_c superconducting cuprates $La_{1.85}Sr_{0.15}CuO_4$ and $YBa_2Cu_3O_7$, the anisotropy in the Fermi velocity is quite large, showing the strong 2D nature in the electronic structure.[11] It turns out that the hexagonal $Ag_5Pb_2O_6$ has less 2D character than the ruthenate and cuprates, despite the layered structure with the 1D chains and 2D kagomé layers of silver.

Hall coefficients are also estimated to be $R^H_{xyz}=-12.6\times10^{-10}$ m^3/C and $R^H_{yzx}=-5.0\times10^{-10}$ m^3/C. Here, the Hall coefficients are defined as $R^H_{\alpha\beta\gamma}=E_\beta/(j_\alpha B_\gamma)$, where j_α is a measured electric current in the presence of an electric field E_β and a magnetic field B_γ. The negative sign of the Hall coefficients means that the carrier is an electron. No Hall measurements have been reported so far.

The temperature dependence of the resistivity may be discussed within the Boltzmann theory if the scattering mechanism is dominated by the electron-phonon coupling. With use of the coupling taken from the experimental phonon spectra, the resistivity in the high-T_c cuprates has been calculated by Allen *et al.*[19,20] and shows a T-linear dependence, which is in good agreement with experiment. For $Ag_5Pb_2O_6$, Yonezawa and Maeno have assumed simple Debye and Einstein model terms in the coupling and reproduced the T^2 dependence of the observed resistivity by adjusting the Debye and Einstein frequencies.[3] However, the Einstein frequency of higher than 1000 K implies the existence of a unique phonon mode for understanding the T^2 dependence within the electron-phonon mechanism.

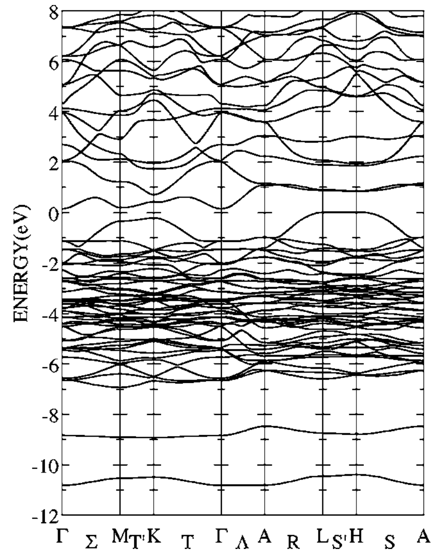

FIG. 8. Calculated energy band structure of Ag_5PbBiO_6. The valence band maximum is taken at the origin.

D. Doping effects

It has been reported that doping of Bi or Cu substituted for the Pb site tends to make the system insulating while In doping shows only a moderate increase in the resistivity.[21,22] A naive interpretation for the insulating state can be made for a composition with one valence electron more or less than that in $Ag_5Pb_2O_6$, such as Ag_5PbBiO_6 and Ag_5PbInO_6, since the conduction band of $Ag_5Pb_2O_6$ is half filled. However, there are no energy gaps below or above the half-filled conduction band as shown in Figs. 2 and 3 and a simple band-filling picture within a rigid-band model cannot seem to explain the insulating nature. Even if there were gaps, it cannot account for the In-doping effect instead. A clue to the convincing explanation is the theoretical finding that the conduction band in $Ag_5Pb_2O_6$ is composed mostly of the antibonding state of Pb 6*s* and O 2*p*, as mentioned above. Substitutional doping for the Pb site may give rise to a crucial modification of the antibonding bands. We have carried out first-principles electronic structure calculations for Ag_5PbMO_6 (M=Bi, In) and results are shown in Figs. 8 and 9. In the calculations, the crystal structure of Ag_5PbMO_6 is assumed to be the same as that of $Ag_5Pb_2O_6$ to see doping effects on the electronic structure. It is found in Ag_5PbBiO_6 (Fig. 8) that there exists one more valence electron occupying the conduction band and energy gaps are clearly formed at the middle of the antibonding bands, of which the lower occupied and upper empty branches are approximately of Bi 6*s* and Pb 6*s* origin, respectively. The gap formation originates in a symmetry lowering by substitutional doping for the Pb site. On the other hand, no gaps are obtained for Ag_5PbInO_6 (Fig. 9) with one less valence electron and the conduction and valence bands overlap each other, leading to

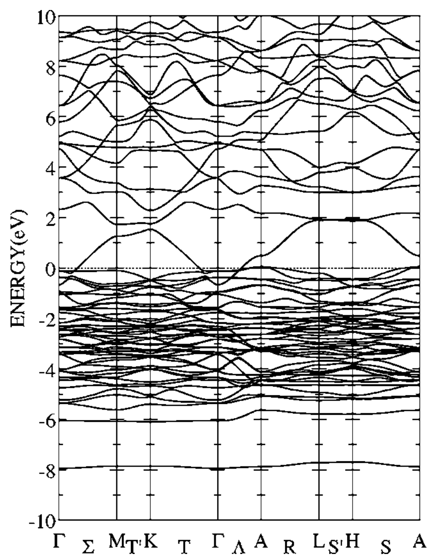

FIG. 9. Calculated energy band structure of Ag_5PbInO_6. The Fermi energy is taken at the origin.

semimetallic electronic structure. These results of the doping effects are quite consistent with the resistivity data.[21,22] It is, furthermore, necessary to elucidate insulating nature in a Cu-doped system.

V. CONCLUDING REMARKS

The electronic band structure is obtained for hexagonal $Ag_5Pb_2O_6$ by first-principles calculations. A half-filled, single conduction band is composed mostly of an antibonding state of Pb 6*s* and O 2*p* with 2D nature and shows dispersion along the *c* direction due to hybridization with the Ag 4*d* and 5*s* orbitals. The resulting Fermi surface has cylindrical shape with large warping along the *c* direction, being regarded possibly as a 3D nearly-free-electron-like one. The anisotropy in the transport properties is expected to be rather small because of comparable Fermi-velocity components parallel and perpendicular to the 2D layer. The observed doping effects on the electronic structure are reasonably understood in terms of the filling and gap formation in the conduction bands.

ACKNOWLEDGMENTS

This work is supported in part by a Grant-in-Aid for Scientific Research in Priority Area (No. 16076212) and COE Research (No. 13CE2002) of the Ministry of Education, Culture, Sports, Science and Technology of Japan. We thank Yoshiteru Maeno, Singo Yonezawa, and Tatsuya Shishidou, for invaluable discussions.

[1] Y. Tokura, *Colossal Magnetoresistive Oxides* (Gordon and Breach, Reading, 2000).
[2] I. Terasaki, *Oxide Thermoelectrics* (Research Signpost, Trivandrum, 2002).
[3] S. Yonezawa and Y. Maeno, Phys. Rev. B **70**, 184523 (2004).
[4] S. Yonezawa and Y. Maeno, cond-mat/0509018 (unpublished).
[5] T. D. Brennan and J. K. Burdett, Inorg. Chem. **33**, 4794 (1994).
[6] I. R. Shein and A. L. Ivanovskiĭ, Phys. Solid State **47**, 599 (2005).
[7] M. B. M. Jansen and K. Heidebrecht, J. Less-Common Met. **161**, 17 (1990).
[8] M. Weinert, J. Math. Phys. **22**, 2433 (1981).
[9] E. Wimmer, H. Krakauer, M. Weinert, and A. J. Freeman, Phys. Rev. B **24**, 864 (1981).
[10] J. M. Soler and A. R. Williams, Phys. Rev. B **40**, 1560 (1989).
[11] T. Oguchi, Phys. Rev. B **51**, 1385 (1995).
[12] K. Iwashita, T. Oguchi, and T. Jo, Phys. Rev. B **54**, 1159 (1996).
[13] T. Shishidou and T. Oguchi, Phys. Rev. B **62**, 11747 (2000).
[14] T. Oguchi and T. Shishidou, Phys. Rev. B **70**, 024412 (2004).
[15] P. E. Blöchl, O. Jepsen, and O. K. Andersen, Phys. Rev. B **49**, 16223 (1994).
[16] J. F. Janak, V. L. Moruzzi, and A. R. Williams, Phys. Rev. B **12**, 1257 (1975).
[17] J. P. Perdew, K. Burke, and M. Ernzerhof, Phys. Rev. Lett. **77**, 3865 (1996).
[18] T. Oguchi and T. Sasaki, J. Phys. Chem. Solids **53**, 1525 (1992).
[19] P. B. Allen, T. P. Beaulac, F. S. Khan, W. H. Butler, F. J. Pinski, and J. C. Swihart, Phys. Rev. B **34**, 4331 (1986).
[20] P. B. Allen, W. E. Pickett, and H. Krakauer, Phys. Rev. B **37**, 7482 (1988).
[21] M. Boltz, M. Jansen, H. Hohl, and E. Bucher, J. Solid State Chem. **103**, 447 (1993).
[22] E. M. Tejada-Rosales, J. Oró-Solé, and P. Gómez-Romero, J. Solid State Chem. **163**, 151 (2002).